Available online at www.sciencedirect.com
SCIENCE DIRECT
Polymer 46 (2005) 10180–10190
polymer
www.elsevier.com/locate/polymer

A comparative study of the structure–property behavior of highly branched segmented poly(urethane urea) copolymers and their linear analogs

Jignesh P. Sheth[a,1], Serkan Unal[b], Emel Yilgor[c], Iskender Yilgor[c], Frederick L. Beyer[d], Timothy E. Long[b], Garth L. Wilkes[a,*]

[a]*Department of Chemical Engineering, Virginia Polytechnic Institute and State University, Blacksburg, VA 24061, USA*
[b]*Department of Chemistry, Virginia Polytechnic Institute and State University, Blacksburg, VA 24061, USA*
[c]*Department of Chemistry, Koc University, Istanbul 34450, Turkey*
[d]*Army Research Laboratory, Materials Division, Aberdeen Proving Ground, Aberdeen MD 21005-5069, USA*

Received 18 March 2005; received in revised form 18 July 2005; accepted 20 July 2005
Available online 10 August 2005

Abstract

The solid-state structure–property behavior of highly branched segmented poly(urethane urea) (PUU) copolymers and their linear analog was investigated. A limited study of their solution rheological behavior was also undertaken. The linear PUUs were synthesized by the two-step prepolymer method, whereas the oligomeric A_2+B_3 methodology was utilized to synthesize the highly branched materials. The soft segments (SS) were either poly(tetramethylene oxide) (PTMO) or poly(propylene oxide) (PPO). All copolymers utilized in this study, with one exception, contained 28 wt% hard segment (HS) content. DMA, SAXS, and AFM studies indicated that the linear as well as the highly branched PUUs were microphase separated. The SS T_g of the highly branched PUUs was nearly identical to that of their respective linear analogs. However, the linear copolymers exhibited broader and less temperature sensitive rubbery plateaus, both attributed to one or both of two reasons. The first is better hydrogen bonding organization of the HS phase as well as greater HS lengths than in the highly branched analogs. The second parameter is that of a potentially higher chain entanglement for the linear systems relative to the branched analogs. Tapping-mode AFM phase images confirmed the microphase morphology indicated by SAXS and DMA. Ambient temperature strain-induced crystallization was observed in the PUU based on PTMO 2040 g/mol at a uniaxial strain of ca. 400%, irrespective of the chain architecture. Stress–strain, stress relaxation, and mechanical hysteresis of the highly branched copolymers were in general slightly poorer than that of their linear analogs. Ambient temperature solution viscosity of the highly branched materials in dimethyl formamide was substantially lower that that of the linear samples of nearly equal molecular weight.

Keywords: Polyurethanes; Highly branched polymers; Atomic force microscopy

1. Introduction

Hyperbranched polymers are typically synthesized by the polymerization of AB_x monomers, where x is 2 or higher. Another approach is the copolymerization of A_2 and B_3 monomers, which is often more attractive due to commercial availability of many A_2 and B_3 monomers. Since their initial discovery, the synthesis of hyperbranched counterparts of almost all common linear polymers has been reported [1–4]. DSM Corporation of The Netherlands recently reported [5] perhaps the first commercialization of hyperbranched polymers, the Hybrane® polyesteramides. These materials are targeted for applications that include improving the dyeability of polypropylene fibers and improving the control of the rheological behavior of paper coating dispersions. However, there are very few reports on the synthesis of hyperbranched systems utilizing the commercially important isocyanate chemistry [6–11]. Spindler and Fréchet [6] reported the first synthesis of

* Corresponding author. Tel.: +1 540 231 5498; fax: +1 540 231 8511.
E-mail address: gwilkes@vt.edu (G.L. Wilkes).
[1] Present address: Xerox Corporation, 26600 SW Parkway Ave., Wilsonville, OR 97070, USA.

0032-3861/$ - see front matter © 2005 Elsevier Ltd. All rights reserved.
doi:10.1016/j.polymer.2005.07.068

hyperbranched polyurethanes wherein they utilized protected or blocked isocyanates. Later, Kumar and Ramakrishnan [7,8] produced wholly aromatic hyperbranched polymers with urethane linkages by the polymerization of 3,5-dihydroxy benzozyl azide. An important observation made by Kumar and Ramakrishnan was that the T_g (measured by DSC) of the hyperbranched polymer without the oxyethylene spacer ($x=0$) was 106 °C and it decreased to 13 °C when the length of the spacer was increased to $x=2$. The degradation temperature on the other hand increased from 240 °C ($x=0$) to 310 °C ($x=2$). The same research group also synthesized hyperbranched polymers with urea linkages [9] by using the polycondensation of 3,5-diaminobenzoylazide monomers. Gao and Yan [10] utilized commercially available A_2 and CB_n ($n=2$ or higher) monomers to produce hyperbranched polymers with urethane and urea linkages. Finally, Bruchmann and Schrepp [11] recently described a one-step methodology for the preparation of hyperbranched poly(urethane urea)s, utilizing commercially available A_2 and B_3 type monomers, where the A_2 monomer was a diisocyanate (isophorone diisocyanate or toluene diisocyanate) and the B_3 monomer was an aminoalkanediol.

The hyperbranched polyurethanes, polyureas, or poly(urethane urea)s discussed above consist only of hard segment (HS) moieties and thus are not segmented, that is, they do not consist of alternating hard and soft segments along the chain backbone. Recently, with the aim of producing branched polymers with a high number of terminal functional groups that also possess useful structural properties, our laboratories reported the synthesis of segmented, highly branched poly(urethane urea)s (PUU) based on the oligomeric A_2+B_3 approach [12]. In that study, isocyanate end-capped poly(tetramethylene oxide) (PTMO) or poly(propylene oxide) (PPO) was utilized as the oligomeric A_2, and tris(2-aminoethyl)amine (TRIS) was used as the B_3 monomer. In the current report, the solid-state structure–property behavior of these PUUs is presented. A limited examination of the solution rheological behavior for these PUUs is also given. First, the highly branched copolymers are compared with their linear, segmented PUU analogs. Second, given the ability of PTMO and the inability of PPO to undergo strain induced crystallization, linear and highly branched PUUs based on PTMO-2040 (MWD 1.87) are compared with those based on PPO-2030 (MWD 1.03). Finally, PUUs containing PPO are used to study the effect of SS entanglements on the structure–property behavior of highly branched PUUs by incorporating several different PPOs (MWD < 1.1) having MWs below and above the critical MW between entanglements, M_c (7700 g/mol [13]). (It is recognized that the M_c values of PTMO and PPO quoted are for homopolymers, and that copolymerization and chain architecture may influence the MW at which SS entanglement is observed.) The samples in this study, with one exception, contain 28 wt% HS. The use of the term 'highly branched', instead of the more common 'hyperbranched', to describe the branched copolymers utilized in this study emphasizes that, for a given overall MW, the use of oligomeric A_2 precursors will inevitably produce copolymers with less branching per unit mass than those that would result from monomeric A_2 precursors.

2. Experimental

2.1. Materials and synthesis

Bis(4-isocyanatocyclohexyl)methane (HMDI) (Bayer MaterialScience) and cyclohexylisocyanate (CHI) (Aldrich) with purities greater than 99.5% were used. Poly(tetramethylene oxide)glycol (DuPont) with $\langle M_n \rangle$ of 2040 g/mol, and poly(propylene oxide)glycols (Bayer MaterialScience) with $\langle M_n \rangle$ values of 2030, 4040, 8000 and 11,800 g/mol were all used as received. The respective hydroxyl numbers were utilized to calculate $\langle M_n \rangle$ of the PTMO and PPO oligomers. 2-Methyl-1,5-diaminopentane (DY) (DuPont), tris(2-aminoethyl)amine (TRIS) (Aldrich), HPLC grade isopropyl alcohol (IPA) (Aldrich) and tetrahydrofuran (THF) (Aldrich) were used as received.

All polymerizations were conducted in three-neck round bottom flasks equipped with an overhead stirrer, addition funnel, and nitrogen inlet. Both linear and highly branched segmented PUU copolymers were prepared in two steps by using the 'prepolymer method'. Prepolymer formation (or isocyanate end-capping) reactions of PTMO and PPO were conducted in bulk at 80 °C with 100 ppm T-12 as the catalyst. Linear polymers were produced by the chain extension of the selected prepolymer with DY at room temperature. Highly branched copolymers were prepared by the slow addition of the isocyanate end-capped prepolymers (A_2) onto triamine (B_3) solution at room temperature. Reaction solvents were IPA and THF/IPA (25/75) for PPO and PTMO based copolymers, respectively. The concentration of the reaction medium was 20% solids for linear copolymers and 10–12% solids for highly branched copolymers. After polymerization, the excess amine groups in all of the highly branched PUUs, except one, were capped with CHI to form urea linkages. These near terminal urea linkages were expected to facilitate inter and intramolecular bidentate hydrogen bonding in these highly branched PUU copolymers. Detailed synthetic procedures are elsewhere [12].

The copolymers utilized in this report, except one, are based on a constant HS content of 28 wt%; HMDI+DY constitute the HS in linear PUUs whereas HMDI+TRIS+CHI comprise the HS in the highly branched analogs. The samples are listed in Table 1 and identified by the nomenclature: SS type and MW-Chain architecture. For example, a linear sample based on PTMO of $\langle M_n \rangle$ 2040 g/mol is identified as 'T2-L' whereas a highly branched sample based on PPO of $\langle M_n \rangle$ 8000 g/mol is identified as 'P8-H'. The molar ratios of precursors, the absolute $\langle M_w \rangle$,

Table 1
Molar composition, weight average molecular weight, and molecular weight distribution of linear and highly branched PUUs based on PPO or PTMO soft segments

Sample	Molar composition (SS/HMDI/amine[a]/CHI)	$\langle M_w \rangle$[b] (g/mol)	M_w/M_n[c]
T2-L	1.0/2.4/1.4/–	220,000	4.41
T2-H	1.0/2.0/1.0/1.0	92,000	5.78
T2-H-no CHI[d]	1.0/2.0/1.0/–		
P2-L	1.0/2.4/1.4/–	45,000	2.59
P2-H	1.0/2.0/1.0/1.0	110,000	7.14
P4-L	1.0/4.5/3.5/–	94,000	2.30
P4-H	1.0/3.7/2.4/2.0	150,000	7.72
P8-L	1.0/8.5/7.5/–	120,000	2.10
P8-H	1.0/6.8/5.3/4.2	76,000	4.11
P12-L	1.0/12.4/11.4/–	77,000	2.18
P12-H	1.0/9.9/8.1/6.5	53,000	4.06

[a] Linear (L) PUU copolymers utilize 2-methyl-1,5-diaminopentane as the amine and the highly branched analogs utilize tris(2-aminoethyl)amine as the amine.
[b] $\langle M_w \rangle$ values are absolute MWs determined by triple angle laser light scattering. The samples were dissolved in hexafluoroisopropanol for measurement.
[c] $\langle M_n \rangle$ values are absolute and were measured by differential viscometry.
[d] The HS content of T2-H-no CHI is 25 wt%.

and the MWD of these copolymers are also listed in Table 1. Equimolar amounts of TRIS and HMDI terminated PPO or HMDI terminated PTMO were utilized to synthesize P2-H and T2-H. However, to maintain a constant HS content of 28 wt%, excess HMDI and TRIS had to be added as the PPO SS MW was raised above 2030 g/mol. The required excess (Table 1) increased with increasing PPO MW. Thus, the extent of HS branching level in a given HS will somewhat increase with PPO MW in the highly branched PUUs.

2.2. Experimental methods

The copolymer films (0.3–0.5 mm thick) utilized for solid-state analyses were cast from IPA solution into poly(tetrafluoroethylene) molds and dried at room temperature overnight. Films were further dried at 65 °C until a constant weight was reached, monitored thermogravimetrically. These films were stored at ambient temperature under vacuum until they were analyzed.

The absolute molecular weight of the samples (Table 1) was determined according to the procedure presented in detail elsewhere [14].

A Seiko Instruments model DMS210 was used for dynamic mechanical analysis (DMA). The film samples, 3–4 mm wide and 10 mm long, were quenched from room temperature to −150 °C using liquid nitrogen and immediately thereafter subjected to a 2 °C/min heating scan under a dry nitrogen atmosphere. tan δ and storage modulus, E', data were obtained at a frequency of 1 Hz.

Ambient temperature tensile testing was conducted using an Instron model 4400R equipped with a 1-kN tension load cell and calibrated with a 2 kg standard (19.61 N). 'Dog-bone' shaped film specimens, 2.9 mm wide and a grip separation distance of 10 mm were used to generate the stress–strain curves at a crosshead speed of 25 mm/min. Three samples were tested for each copolymer and the average Young's modulus of these three runs is reported. Only representative stress–strain responses are presented in the appropriate figure. Stress relaxation studies were also performed on similar dog-bone shaped specimens at strain levels of 25 or 500%. Mechanical hysteresis experiments were also performed at strain levels of 25 or 500% for two uniaxial deformation cycles each and at a crosshead speed of 25 mm/min.

Pin-hole collimated small angle X-ray scattering (SAXS) data were collected at ambient temperature using a Rigaku Ultrax18 rotating anode X-ray generator operated at 40 kV and 60 mA. A pyrolytic graphite monochromator was used to filter out all radiation except the Cu K_α doublet, with an average wavelength of 1.5418 Å. The camera used 200, 100 and 300 μm pin-holes for X-ray collimation. Two-dimensional data sets were collected using a Molecular Metrology 2D multi-wire area detector, located approximately 65 cm from the sample. After azimuthal averaging, the raw data were corrected for detector noise, absorption, and background noise [15]. The data were then placed on an absolute scale using a type 2 glassy carbon sample 1.07 mm thick, previously calibrated at the advanced photon source in the Argonne National Laboratory, as a secondary standard [16].

A Digital Instruments (now Veeco) Dimension 3000 scanning probe microscope controlled by a Nanoscope IIIa controller, was utilized for tapping-mode atomic force microscopy (AFM). Images of the free surface of thoroughly dried solution cast films were captured at a magnification of $2\times2\ \mu m^2$ and a set-point ratio of approximately 0.6. Nanosensors' TESP 7 or Veeco's TAP 300 tips having a spring constant of 35–40 N/m were utilized for imaging.

TA Instruments AR1000 rheometer with 2°, 40 mm diameter cone-and-plate attachment was used to measure the viscosity of 15 wt% copolymer solutions in dimethyl formamide at room temperature. The solution viscosity of a sample was determined from the initial slope of shear stress versus shear rate within the Newtonian or linear region of this plot. The reported viscosity numbers are averages of 3–4 repeat runs per sample.

3. Results and discussion

3.1. Dynamic mechanical analysis

The storage modulus, E' and tan δ responses as functions of temperature for both linear and highly branched PUUs based on PTMO and PPO are presented in Fig. 1. The DMA behavior of PTMO-2000 based copolymers presented in Fig. 1(a) is addressed first. Focusing on E' of the linear

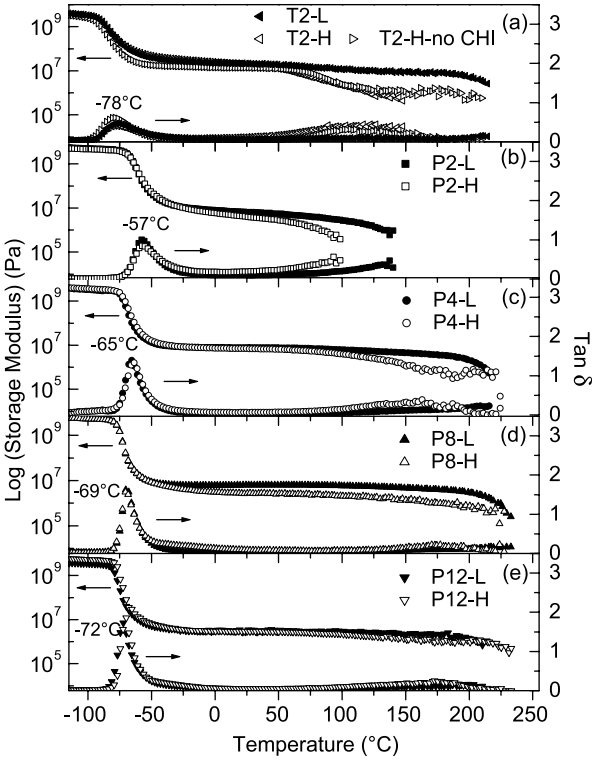

Fig. 1. DMA response of linear and highly branched PUUs (a) T2-L and T2-H; (b) P2-L and P2-H; (c) P4-L and P4-H; (d) P8-L and P8-H; (e) P12-L and P12-H.

sample, T2-L behaves as a rigid solid up to ca. −100 °C. Thereafter, E' begins to decrease due to the glass transition of the PTMO SS (T_g −78 °C, tan δ peak value). Not surprisingly, the SS T_g is slightly higher than that of the pure PTMO oligomer (−85 °C [17]) due to restrictions experienced by the SS from the covalently linked urea HS and any isolated HS potentially dissolved in the soft matrix. After the SS glass transition induced, a relatively temperature insensitive rubbery plateau can be observed that extends up to 200 °C. As is well known, in structural applications, this plateau is also referred to as the 'service window' of the copolymer. Finally, another drop in E' occurs due to the softening of the hard phase. The low T_g of the SS coupled with the broad and nearly temperature insensitive rubbery plateau indicate that the sample possesses a microphase morphology. From the tan δ behavior of this sample, two distinct transitions can be noted that correspond to the respective transitions in E'. A damping peak centered at −78 °C occurs due to the SS glass transition. An increase in tan δ values is noted above 200 °C due to the softening of the hard phase and possible onset of degradation of the material since it is known [18] that both urethane and urea linkages are not highly stable for long periods in the range of 200 °C.

The DMA behavior of the PTMO based highly branched analog, T2-H is also presented in Fig. 1(a). Interestingly, below 50 °C the E' and tan δ responses of T2-H are very similar to T2-L. The former sample also displays a drop in E' from ca. −100 to −50 °C due to the SS glass transition and a rubbery plateau extends thereafter. The average plateau moduli of both samples are also comparable up to 50 °C. However, the rubbery plateau is significantly narrower in T2-H than it is in T2-L. The narrower rubbery plateau of T2-H is expected to arise due to (1) the lower $\langle M_w \rangle$ of T2-H as compared to T2-L (recall Table 1); this will lead to a lower number of entanglements per chain, (2) difficulty in the hydrogen bonding/organization (or packing) of branched HS in T2-H, and (3) slightly shorter average length of the HS in the branched architecture. The shorter average HS length, and the branched structure of HS in T2-H is expected to promote increased intersegmental mixing and therefore contribute to a narrower rubbery plateau. This last observation follows from the expectation that T2-H should have slightly shorter HS than T2-L because the HS content of the highly branched samples is calculated by assuming the terminal end-capping moieties, namely CHI, to be part of the HS. From the tan δ response of T2-H, it can be again noted that the breadth of the SS glass transition and the peak transition temperature, T_g (−78 °C) are very similar to T2-L. However, due to reasons noted above, the rise in tan δ, which corresponds to the decrease in E' occurs at a lower temperature (ca. 50 °C) than in T2-L (200 °C).

In Fig. 1(a), the DMA response of the CHI end-capped T2-H (28 wt% HS content) is compared with its counterpart, that is, without the end-cap moiety (T2-H no CHI, 25 wt% HS content). Despite the slightly lower HS content and the likely reduced, if any, intermolecular bidentate hydrogen bonding of the latter, no significant differences are noticeable between the two highly branched PTMO-2040 based samples.

Turning attention to Fig. 1(b), the DMA behavior of PPO-2030 based linear and highly branched samples is very similar to that of the corresponding PTMO-2040 based samples presented in Fig. 1(a). However, some noteworthy differences can also be observed. First, the PPO SS T_g occurs at −57 °C as compared to the PTMO SS T_g at −78 °C, principally due to differences in the chemical structures of the two types of SS and also due to potential differences in the extent of microphase separation (see below). The T_g of the pure PPO oligomers is reported to be approximately −73 °C [19] whereas that of the PTMO oligomers is −85 °C [17]. Second, the average rubbery plateau modulus of the PTMO based copolymers is nearly three times that of the PPO based materials. This difference is believed to be due to the higher entanglement density in the PTMO-2040 segments as compared to the PPO-2030 segments. The M_c of PTMO is 2500 g/mol whereas for PPO it is significantly higher, 7700 g/mol [13]. This result underscores the importance of the SS MW in relation to M_c as a means of controlling the stiffness of the copolymer within its rubbery plateau region. Tong and Jerome [20] also note that in tri-block copolymers, such as poly(methyl methacrylate)-*b*-poly(alkyl acrylate)-*b*-poly(methyl methacrylate) and polystyrene-*b*-polyisoprene-*b*-polystyrene of

comparable hard block content (ca. 30 wt%), the entanglements of the central soft block play a critical role in governing the tensile strength of the material. Finally, the rubbery plateau of the PTMO-2040 based samples is significantly broader than that of the PPO-2030 based counterparts possibly because the overall $\langle M_w \rangle$ of P2-L and P2-H is substantially lower than that of T2-L (recall Table 1).

Considering the series of copolymers based on PPO, note that the overall $\langle M_w \rangle$ of these copolymers (Table 1), with the exception of P2-L and P12-H, is comparable and in the range of 100,000 g/mol. Schollenberger and Dinbergs [21] note that the mechanical properties of linear segmented polyurethanes reach a plateau value around $\langle M_w \rangle$ between 100,000 and 200,000 g/mol. The differences in E' and tan δ responses between the PPO based linear PUU and its highly branched analog also arise due to similar reasons as discussed above. When the MW of the PPO SS is increased from 2030 to 4040, 8000 and finally to 11,800 (Fig. 1(c)–(e)), a systematic decrease in the SS T_g and also the breadth of the SS glass transition are observed (from both the E' and tan δ responses) with increasing PPO MW. This trend results because when the HS content of the copolymers is maintained constant, the longer SS experience fewer restrictions, which therefore form fewer junctions with the HS. O'Sickey et al. [22] have also observed similar behavior in poly(urethane urea)s based on PPO of narrow MWD (<1.03). In the linear PUUs shown in Fig. 1(c)–(e), as the PPO SS MW in increased, the rubbery plateaus become less temperature sensitive and extend to higher temperature (ca. 200 °C) primarily due to an improved extent of microphase separation (discussed below). In comparison to the linear PUUs, the rubbery plateau of the highly branched analogs based on PPO-4040 and PPO-8000 begins to decay earlier due to their branched architecture, shorter HS length as compared to their linear analogs, and potentially lower extent of microphase separation. Of particular interest is the observation that the breadth of the rubbery plateau of P12-H is nearly comparable to its linear analog, P12-L. The fact that the SS MW in these two copolymers is well above the M_c of PPO may be responsible for such behavior. Another important reason why the rubbery plateau of P12-H is comparable to P12-L is the low $\langle M_w \rangle$ of P12-H (53,200 g/mol), which means that the degree of branching in this sample is only modest.

3.2. Small angle X-ray scattering

The pin-hole collimated ambient temperature SAXS profiles of PPO and PTMO based linear and highly branched PUU copolymers are presented in Fig. 2. The corrected intensities are plotted as a function of the scattering vector, s, where $s=2\sin(\theta/2)/\lambda$, θ is the radial scattering angle and wavelength $\lambda=1.542$ Å. The scattering profiles of all 11 samples exhibit distinct first-order interference peaks. The SAXS data suggest that all the samples in this study possess a microphase separated morphology, consistent with the respective ambient temperature DMA responses. The interdomain spacing of a given sample, approximately $1/s_{max}$, according to Bragg's Law, is noted in the legends in Fig. 2.

The SAXS data for the linear PUUs based on PPO are presented in Fig. 2(a). From this figure it can be observed that with increasing SS MW, the interdomain spacing increases from approximately 80 Å for P2-L to 145 Å for P12-L. The absolute intensity of the first order interference peak also increases with SS MW, although this behavior is not readily apparent because the SAXS profiles have been translated vertically for clarity. Simultaneously, the breadth of the first-order interference peak decreases systematically with increasing SS MW. However, direct comparison of the peak breadth is not warranted since the abscissa (namely, 's') is non-linear with respect to the structural scale length (Bragg spacing).

Focusing on the SAXS data for the microphase separated highly branched PUUs based on PPO, presented in Fig. 2(b), several remarkable features can be noted. First, a marked systematic narrowing of the breadth of the first order interference peak is observed. This trend is consistent with the behavior of the linear PUU samples. Second, the position of the first-order interdomain interference peak shifts generally to lower angles with increasing SS MW, as observed for the linear PUU samples. The only exception to this trend is found for sample P12-H, with a domain spacing of 179 versus 196 Å for sample P8-H. The underlying reasons for such behavior are not understood at this point but the data have been reconfirmed.

Finally, a distinct apparent weak higher order interference shoulder occurs in the scattering profiles of P8-H and P12-H (see arrows in Fig. 2(b)). In both samples, the position of the higher order reflection corresponds to a 'd' spacing that is half the spacing of the corresponding first-order interference peak. Kinning and Thomas [23] have shown that in some diblock copolymers, such as those based on polystyrene-polybutadiene, a second peak or shoulder of weak intensity in the SAXS profile may not truly be a second order interference peak but can arise from 'liquid-like' packing of the nearly spherical hard domains. As will be shown below, the phase images P8-H and P12-H exhibit particulate hard domains. These hard domains also exhibit limited short-range order, especially in P8-H. However, in light of the Kinning and Thomas' work, it is difficult to describe the presence of a second order interference shoulder in the SAXS profiles of P8-H and P12-H as a signature of long-range order. It is also worthwhile to note that an extensive review of the literature conducted by Ryan et al. [24] found no instance of a linear segmented polyurethane exhibiting second- or higher order reflection in SAXS. In that publication, the theoretical work of Fredrickson et al. [25,26] was also referenced, which predicts that random length block copolymer materials,

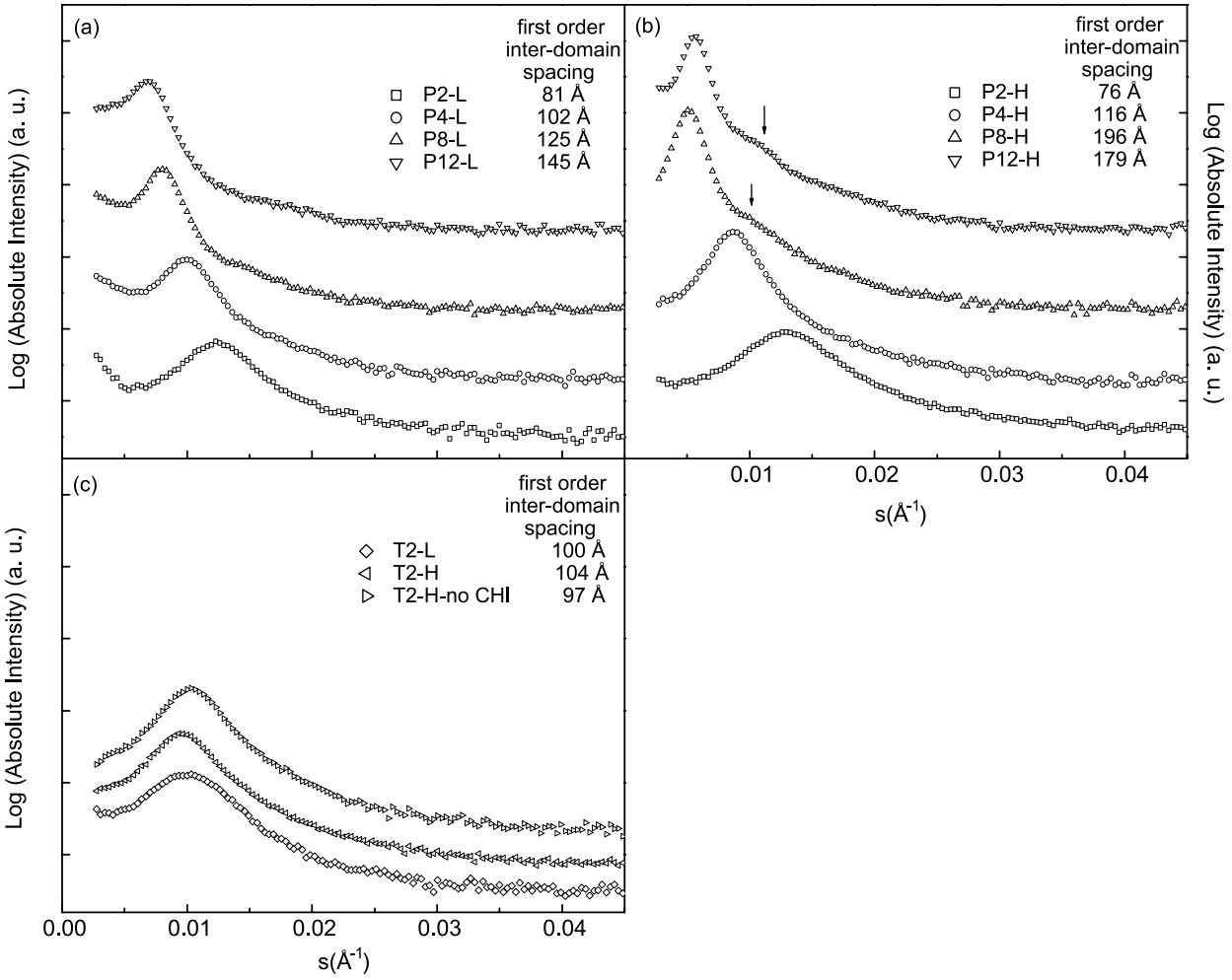

Fig. 2. Pin-hole collimated SAXS profiles of PPO-2030 based linear (a) and highly branched (b) PUUs, and also PTMO-2040 based PUUs (c). Note: The scattering intensity of each profile is absolute but the individual profiles have been translated vertically for clarity. All the SAXS profiles have been masked in the low scattering vector region where the beam stop influenced the profiles.

such as often produced by step-growth polymerization, will lack long-range order due to a broader distribution of the segment lengths. However, some possible exceptions to his analysis have been reported [27–30].

The SAXS profiles of the three PTMO based linear and highly branched PUUs are presented in Fig. 2(c). These three samples also exhibit first-order interference peaks, which again indicate microphase separated morphologies. The interdomain spacing of these PTMO-2000 based samples is higher than that of the PPO-2030 counterparts in Fig. 2(a) and (b). This difference can be attributed to the difference in the average number of bonds along the backbone of PTMO-2040 (142) and PPO-2030 (105) and the unperturbed chain dimensions between PTMO and PPO of comparable average MW, as well as the broader MWD of the PTMO segments (1.87) as compared to the PPO segments (<1.03). O'Sickey et al. [22] have also observed similar differences in the interdomain spacing in linear PUUs based on PPO of narrow MWD (<1.03) and PTMO with a broader MWD (ca. 2).

3.3. Atomic force microscopy

Both DMA and SAXS data indicate that the segmented PUUs addressed in this study possess a microphase morphology at ambient temperature. In addition, the ambient temperature morphology of these copolymers is especially amenable to investigation by tapping-mode AFM. The phase images of the free surface of solution cast PPO-based PUUs captured at ambient temperature are presented in Fig. 3. The dark and the light regions correspond to soft and hard domains, respectively, and all eight PPO-based highly branched PUU samples show separate regions of light and dark indicative of a microphase separated morphology, in agreement with the SAXS and DMA data. Beginning with samples P2-L and P2-H, in Fig. 3(a) and (b), respectively, the morphology seems best characterized as microphase separated but disordered. The phase image of the P4-L (Fig. 3(c)) is very similar to P2-L. On the other hand, the hard domains in sample P4-H (Fig. 3(d)) appear to adopt a more short rod-like shape.

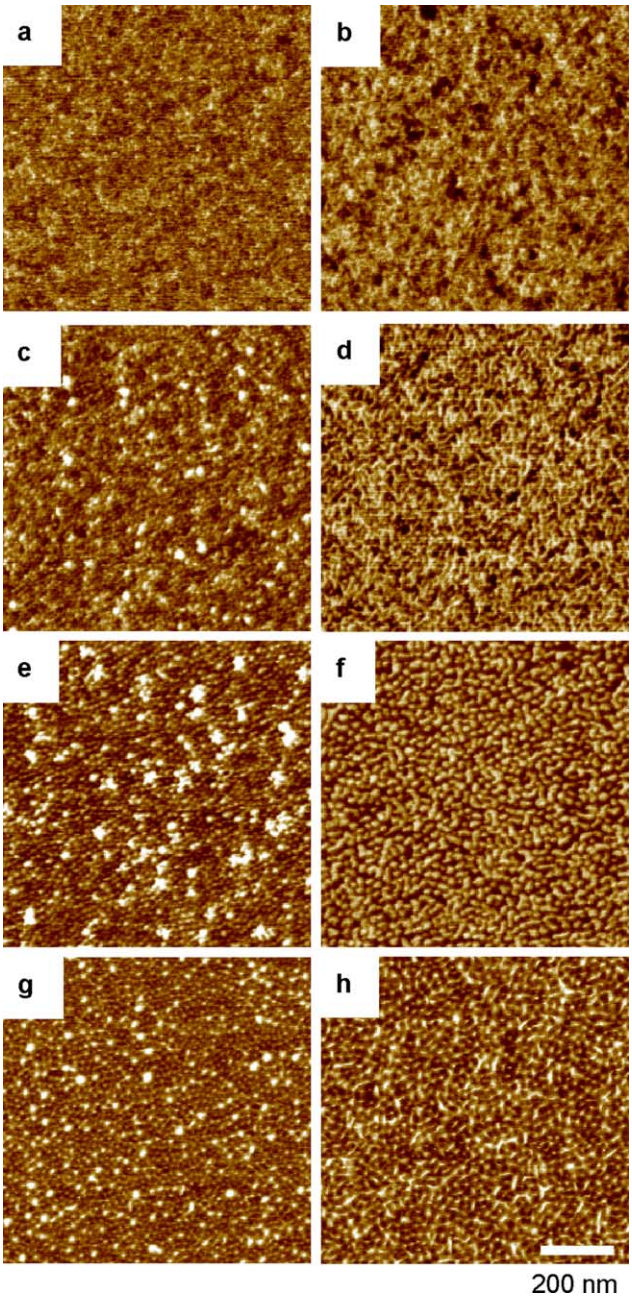

Fig. 3. AFM phase images of the free surface of linear and highly branched PUUs (a) P2-L; (b) P2-H; (c) P4-L; (d) P4-H; (e) P8-L; (f) P8-H; (g) P12-L; and (h) P12-H. Note: The length of the magnification bar corresponds to 200 nm.

While the hard phase in this sample may at first appear to possess considerable degree of hard phase percolation, as will be shown later, its corresponding stress–strain curve does not exhibit any yielding behavior, strongly suggesting that the hard phase in P4-H is not percolated throughout the matrix.

Fig. 3(e)–(h) show AFM images for samples P8-L, P8-H, P12-L, and P12-H, respectively. In general, the hard domains in these samples appear to be spherical or particulate-like. The phase image of the sample P8-H (Fig. 3(f)) is particularly striking. For clarity, the same image as Fig. 3(f) is reproduced at higher magnification in Fig. 4, along with the SAXS profile (from Fig. 2(b)) as an inset. The spherical, particulate nature of the hard domains is apparent, and the average spacing between the domains is approximately 200 Å, which corresponds well with the first-order SAXS interference peak (196 Å). Moreover, from this image the presence of limited short-range order in the hard domain packing can be observed. The sample P12-H also exhibits similar morphology as seen from Figs. 2(b) and 3(h).

3.4. Mechanical properties

In this section, the stress–strain response, the extent of stress relaxation, and the mechanical hysteresis behavior of the linear and highly branched PUU copolymers are presented and compared. The stress–strain results of the PTMO and PPO-based samples are presented in Fig. 5(a) and (b). The Young's moduli of these samples are listed in Table 2. Focusing on Fig. 5(a), the samples T2-L and T2-H display no distinct yield point, which strongly suggests that in these particular systems, 28 wt% HS is insufficient to enable extensive percolation of the hard phase. The AFM images of the PPO-2030 based samples also indicated insufficient percolation of the hard phase. The Young's modulus of T2-L (listed in Table 2) is, surprisingly, lower than T2-H. However, the highly branched copolymer without end-capping, T2-H-no CHI, displays the lowest Young's modulus amongst the three PTMO-based copolymers due to the potentially lower extent of intermolecular bidentate hydrogen bonding and the slightly lower HS content in this sample (25 wt%) as compared to T2-L and T2-H (28 wt%). The strain hardening at higher extensions noted in the linear sample T2-L, undoubtedly occurs due to the well know ability of PTMO (MW > ca. 1500 g/mol) to strain-induce crystallize at greater than approximately 400% strain. WAXS was utilized to investigate the similar strain hardening behavior exhibited by the highly branched sample T2-H. The 2D ambient temperature WAXS pattern (Fig. 6) of T2-H uniaxially deformed to 400% strain demonstrates two distinct equatorial reflections at '*d*' spacings of ca. 4.5 and 3.3 Å, which are due to the

Table 2
Young's moduli of linear and highly branched PUUs determined at ambient temperature

Sample	Young's modulus[a] (MPa)	Sample	Young's modulus[a] (MPa)
T2-L	7.5	T2-H	10.3
		T2-H-no CHI	6.4
P2-L	2.8	P2-H	1.3
P4-L	4.3	P4-H	3.2
P8-L	3.5	P8-H	1.0
P12-L	1.5	P12-H	1.1

[a] The Young's modulus values are averages of three repeat runs. The standard deviation in Young's modulus is less than ±10%.

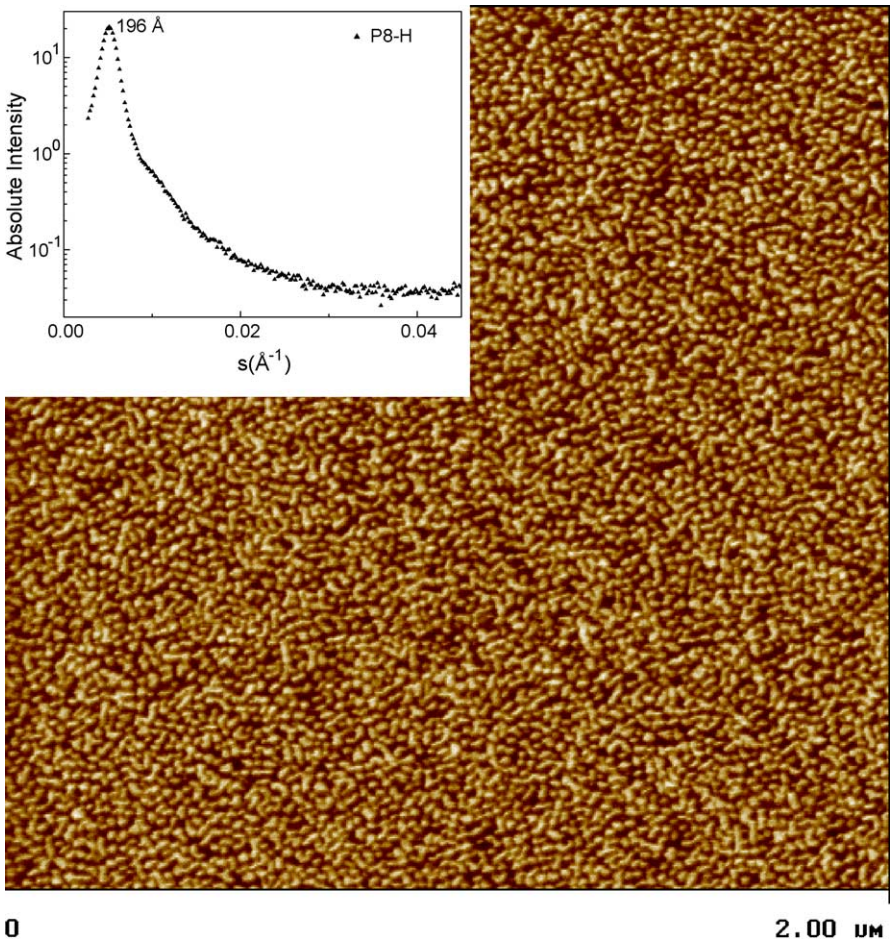

Fig. 4. AFM phase image of the free surface of the highly branched PUU, P8-H. The pin-hole collimated SAXS profile of P8-H is included in the inset.

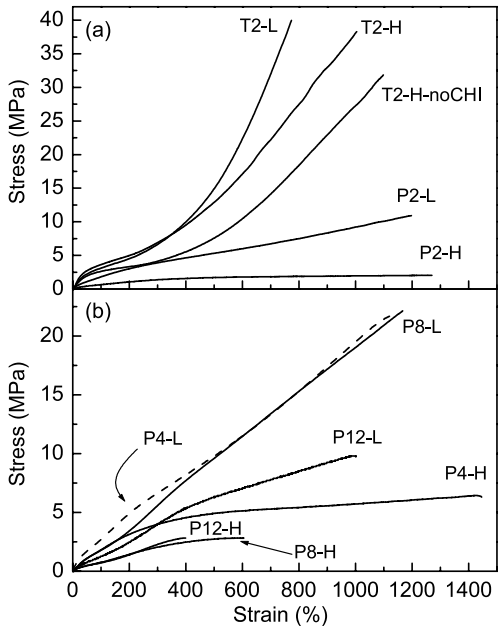

Fig. 5. Stress–strain behavior of linear and highly branched PUUs based on PPO-2030 and PTMO-2040 (a), and PPO of MW 4040, 8000 and 11, 800 g/mol (b).

crystalline PTMO phase [31]. Therefore, the strain hardening behavior of the sample, T2-H-no CHI, is also expected to arise due to the strain-induced crystallization of the PTMO phase, as was also noted in T2-H.

In addition, the tensile strength of T2-L is higher than that of T2-H and T2-H-no CHI, possibly due to the

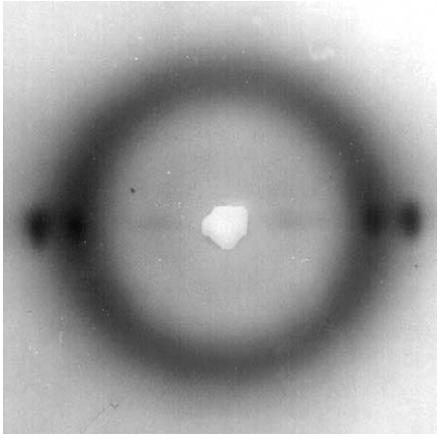

Fig. 6. Wide angle X-ray scattering pattern of the sample, T2-H deformed uniaxially at ambient temperature to ca. 400% strain. The deformation direction is vertical.

substantially higher overall $\langle M_w \rangle$ of T2-L. However, both highly branched samples display a slightly higher elongation at break. Furthermore, while the DMA and SAXS behavior of the samples T2-H and T2-H-no CHI are very similar, the Young's modulus and tensile strength of T2-H are higher than those of T2-H-no CHI. This behavior highlights the benefit of end-capping the chain ends with a moiety that can facilitate intermolecular bidentate hydrogen bonds for structural applications.

The stress–strain behavior of samples P2-L and P2-H is presented in Fig. 5(a). As expected, these two samples, like their PTMO counterparts, do not display a distinct yield point. In addition, the inability of the atactic PPO SS to strain induce crystallize and their comparatively lower overall $\langle M_w \rangle$ (Table 1) results in copolymers with lower tensile strength as compared to the PTMO based copolymers. However, both P2-L and P2-H display a remarkably high strain at break, approximately1200%. The PPO-4040 and 8000 based materials (Fig. 5(a) and (b)) display generally superior Young's modulus (values listed in Table 2), tensile strength, and elongation at break amongst the series. While the overall $\langle M_w \rangle$ of the linear copolymers influences the ultimate properties of the samples, the improved stress–strain behavior of the PPO-4040 and 8000 based samples in comparison to the PPO-2030 and 11,800 based counterparts is not fully understood at this point. However, as expected, the tensile performance of the linear copolymers is distinctly superior to that of their highly branched analogs.

Stress relaxation of the copolymers is another mechanical property of practical interest for systems intended for structural applications. In light of the highly branched copolymers' greater difficulty to entangle, the extent of stress relaxation in these materials is expected to be higher than in their linear analogs. The extent of stress relaxation of the copolymers addressed in this report is presented in Fig. 7. Stress relaxation is quantified as the ratio of the absolute decrease in the stress at $t = 10{,}000$ s (ca. 3 h) to the stress recorded immediately after the sample was first stretched. The samples were uniaxially deformed to 25 or 500% strain and different samples were used for each test. A crosshead speed of 150 mm/min was utilized to reach the required strain. As expected, at both strain levels the extent of stress relaxation of T2-H and T2-H-no CHI is higher than in the linear analog, T2-L. In addition, due to the absence of the end-capping moieties (CHI), which results in a reduced level of intermolecular hydrogen bonding in T2-H-no CHI, it displays higher stress relaxation than the CHI end-capped T2-H. A comparison of the samples T2-L and T2-H with P2-L and P2-H reveals that due to the ability of PTMO to strain induce crystallize both, T2-L and T2-H relax a smaller extent relative to P2-L and P2-H. Amongst the PPO based samples, at 25% strain the extent of stress relaxation exhibited by the highly branched PUUs is generally higher than the linear analogs. At 500% strain, a similar trend can be observed in the PPO-2030 and 4040 based copolymers. The sample, P8-H failed ca. 1000 s after it was stretched to 500% strain, and the stress relaxation of P12-H could not be measured because its strain at break is less than 500% (recall Fig. 5).

The mechanical hysteresis behavior of materials is also of practical importance and it was utilized to further

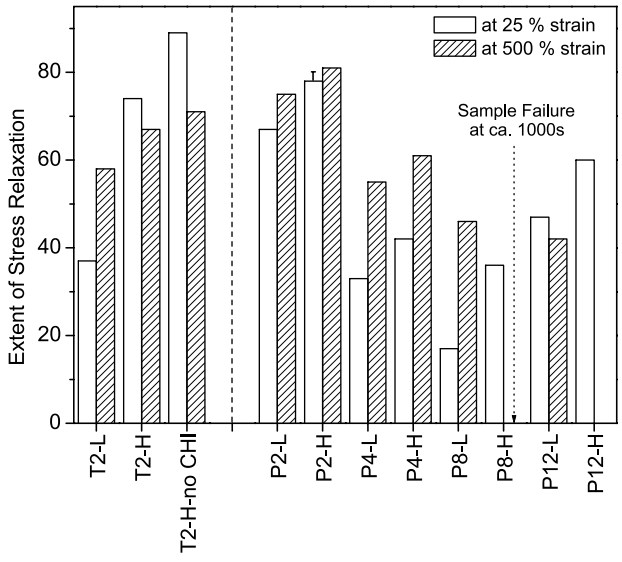

Fig. 7. Extent of ambient temperature stress relaxation in linear and highly branched PUUs uniaxially elongated to 25 and 500% strain.

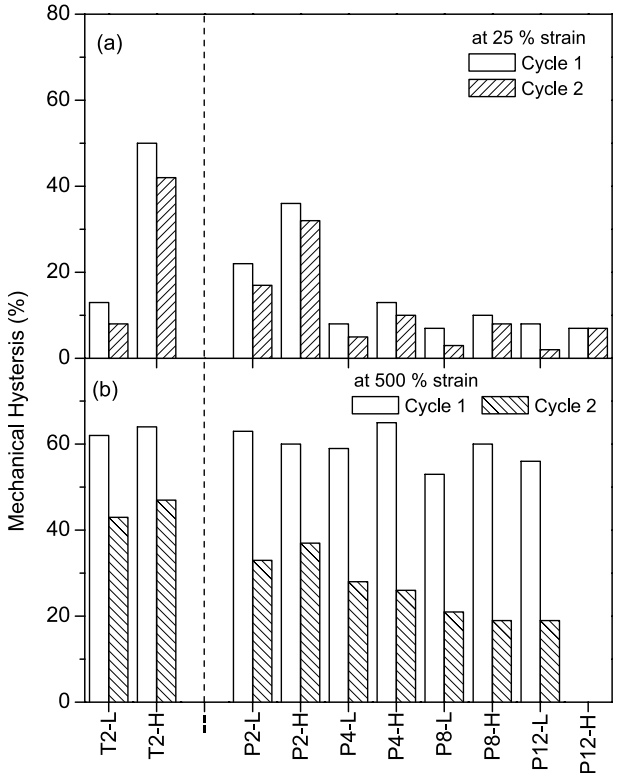

Fig. 8. Ambient temperature mechanical hysteresis of linear and highly branched PUUs during cyclic deformation to 25 or 500% strain. Note: Cycle 2 was initiated immediately after the completion of Cycle 1.

compare the linear segmented PUUs with their highly branched analogs. The mechanical hysteresis of the PTMO and PPO based copolymers during two consecutive cycles to 25 or 500% strain is presented in Fig. 8(a) and (b), respectively. In general, at both strain levels the mechanical hysteresis during cycle 1 is greater than during cycle 2. Such behavior is not surprising because once the original microstructure becomes partially disrupted during the first cycle it does not have enough time to completely 'heal' before the next cycle is initiated. The mechanical hysteresis of linear PTMO-2040 and PPO-2030 based PUUs at 25% strain is, as expected, distinctly lower than their highly branched analogs. However, for the other PPO based materials the difference in the mechanical hysteresis between the linear and highly branched samples appears to be similar. Surprisingly, at 500% strain (Fig. 8(b)) the percent mechanical hysteresis of the linear materials and their highly branched analogs are comparable. Such behavior indicates that the substantial disruption of the microstructure upon deforming the copolymers to 500% strain apparently overrides differences in the entanglement density between the linear and highly branched materials. At 500% strain, despite the ability of the PTMO to strain-induce crystallize, the samples T2-L and T2-H display mechanical hysteresis that is comparable to P2-L and P2-H—this seems a bit surprising to the authors, but the results have been reconfirmed.

3.5. Solution viscosity and implications for processability

The above discussion on the comparison of the mechanical properties of the copolymers indicates that the tensile performance of the highly branched PUUs is generally lower than analogous linear PUUs with identical SS MW and overall HS content. The difficulty of the highly branched architecture to entangle to the same degree as their linear analogs is undoubtedly a major reason for such a difference in tensile properties. However, it is well known that in dilute solutions, the hydrodynamic volume of a branched polymer is lower than that of a linear polymer of comparable MW. In addition, when the concentration of the polymer solution is increased such that it is in the semi-dilute regime where chain overlap is expected, the lower entanglement density of branched polymers also lowers the viscosity of the polymer. Since a material of lower viscosity can be more easily processed, controlled incorporation of branching can be utilized to improve the processability of polymers. The effect of architecture on viscosity was investigated by using a cone-and-plate rheometer to measure the ambient temperature solution viscosity of selected PUUs addressed in this report. The results are presented in Table 3.

The Newtonian (zero shear) solution viscosity of a sample was determined from the initial slope of the linear region of the shear stress versus shear rate plot. The upper shear rate limit of this linear region (before the onset of shear thinning) is also listed in Table 3. The PTMO based linear sample was too viscous for the torque bar of the instrument to measure. In light of its substantially high overall $\langle M_w \rangle$ such behavior is not surprising. However, the solution viscosity of T2-H was measured to be 410 mPa s. The lower solution viscosity of T2-H is believed to be primarily due to the reduced entanglements of its highly branched molecules. The lower overall $\langle M_w \rangle$ of T2-H is also expected to be a contributing factor. On the other hand, the solution viscosity of the linear samples based on PPO-2030 as well as PPO-4040 is higher than the viscosity of the respective highly branched analogs despite the significantly higher $\langle M_w \rangle$ of the branched systems. Such behavior provides further support to the argument that polymer chains with a highly branched architecture encounter considerable difficulty to entangle in the semi-dilute regime and consequently the reduced entanglement density of the highly branched polymers lowers their solution viscosity.

Table 3
Ambient temperature solution viscosity of selected linear and highly branched PUUs

Sample	$\langle M_w \rangle$ (g/mol)	Solution viscosity (mPa s)	Shear stress (mPa) linear up to shear rate (1/*s*)
T2-L	220,000	Very viscous	–
T2-H	92,000	410	500
P2-L	45,000	79	3000
P2-H	110,000	30	3000
P4-L	94,000	1840	40
P4-H	150,000	51	3000
P12-L	77,000	550	80
P12-H	53,000	27	3000

The $\langle M_w \rangle$ values are reproduced from Table 1. The solution viscosity values are averages of three to four repeat runs. The standard deviation is less than $\pm 7\%$.

4. Conclusions

The solid-state structure–property behavior of highly branched segmented PUUs was compared with their linear analogs. DMA, SAXS, and AFM were used to demonstrate that all the copolymers investigated in this report possessed a microphase separated morphology. From the DMA results it was also noted that despite the incorporation of branching, that is, HS branching, the breadth of the SS glass transition and the SS T_g (and therefore, the extent of microphase separation) of the highly branched PUUs was very similar to their linear analogs. Such behavior is consistent with the results presented in an earlier publication from our laboratory [32] wherein increasing extent of HS branching was introduced in model PUUs having a constant 22 wt% HS content.

The strain-induced crystallization of the SS phase in the PTMO-2040 based highly branched PUU at ambient temperature was another noteworthy result. Due to such behavior, the stress–strain response of the highly branched

PUU was comparable to its PTMO-based linear analog. The stress–strain response of the sample not end-capped with CHI was markedly poorer than its linear analog, even though strain hardening could still be observed in the sample that was not end-capped.

The stress–strain response of the PTMO or PPO based copolymers did not exhibit any yield point, thereby suggesting that at 28 wt% HS content there was insufficient percolation of the hard phase through the soft matrix, a fact confirmed by AFM. The stress–strain response, the extent of stress relaxation, and the mechanical hysteresis of the highly branched PUUs were poorer in comparison to their linear analogs, there being one exception. Surprisingly, the mechanical hysteresis of the highly branched PUUs at high deformation (500% strain) was comparable to the linear samples.

Limited ambient temperature solution rheological experiments indicated that the highly branched PUUs had significantly lower viscosity than their linear analogs of nearly equal molecular weight.

Acknowledgements

This material is based upon work supported by the US Army Research Laboratory and the US Army Research Office under grant number DAAD19-02-1-0275 Macromolecular Architecture for Performance (MAP) MURI. The authors also gratefully acknowledge Thomas Mourey of Eastman Kodak Company for measuring the molecular weights of the copolymers utilized in this study, and Charles E. Frazier of Virginia Tech for facilitating the use of his laboratory's cone-and-plate rheometer.

References

[1] Kim YH, Webster OW. Polym Prepr 1988;29:310–1.
[2] Kim YH. J Polym Sci, Part A: Polym Chem 1998;36:1685–98.
[3] Voit B. J Polym Sci, Part A: Polym Chem 2000;38:2505–25.
[4] Jikei M, Kakimoto M. Prog Polym Sci 2001;26:1233–85.
[5] Froehling P. J Polym Sci, Part A: Polym Chem 2004;42:3110–5.
[6] Spindler R, Fréchet JMS. Macromolecules 1993;26:4809–13.
[7] Kumar A, Ramakrishnan S. J Chem Soc Chem Commun 1993; 1453–4.
[8] Kumar A, Ramakrishnan S. J Polym Sci, Part A: Polym Chem 1996; 34:839–48.
[9] Kumar A, Meijer EW. Chem Commun 1998;1629–30.
[10] Gao C, Yan D. Macromolecules 2003;36:613–20.
[11] Bruchmann B, Schrepp W. e-Polymers 2003;014.
[12] Unal S, Yilgor I, Yilgor E, Sheth JP, Wilkes GL, Long TE. Macromolecules 2004;37:7081–4.
[13] Zang YH, Carreau PJ. J Appl Polym Sci 1991;42:1965–8.
[14] Mourey TH, Bryan TG. J Chromatogr A 2002;964:169–78.
[15] Glinka CJ, Barker JG, Hammouda B, Krueger S, Moyer JJ, Orts WJ. J Appl Cryst 1998;31:430–45.
[16] Russell TP, Lin JS, Spooner S, Wignall GD. J Appl Cryst 1988;21: 629–38.
[17] Faucher JA, Koleske JV. Polymer 1968;9:44–7.
[18] Hepburn C. Polyurethane elastomers. New York: Applied Science Publishers; 1992.
[19] Johari GP, Hallbrucker A, Mayer E. J Polym Sci, Part B: Polym Phys 1988;26:1923–30.
[20] Tong JD, Jerome R. Macromolecules 2000;33:1479–81.
[21] Schollenberger CS, Dinbergs K. Adv Urethane Sci Technol 1979;7: 1–34.
[22] O'Sickey MJ, Lawrey BD, Wilkes GL. J Appl Polym Sci 2003;89: 3520–9.
[23] Kinning DJ, Thomas EL. Macromolecules 1984;17:1712–8.
[24] Ryan AJ, Macosko CW, Bras W. Macromolecules 1992;25:6277–83.
[25] Fredrickson GH, Milner ST. Phys Rev Lett 1991;67:835–8.
[26] Fredrickson GH, Milner ST, Leibler L. Macromolecules 1992;25: 6341–54.
[27] Smith SD, DeSimone JM, Huang H, York G, Dwight DW, Wilkes GL, et al. Macromolecules 1992;25:2575–81.
[28] Feng D, Wilkes GL, Crivello JV. Polymer 1989;30:1800–13.
[29] Crivello JV, Lee JL, Conlon DA. J Polym Sci, Part A: Polym Chem 1986;24:1251–79.
[30] Crivello JV, Conlon DA, Lee JL. J Polym Sci, Part A: Polym Chem 1986;24:1197–215.
[31] Tadokoro H. Structure of crystalline polymers. New York: Wiley Interscience; 1979.
[32] Sheth JP, Wilkes GL, Fornof AR, Long TE, Yilgor I. Macromolecules 2005;38:5681–5.